Iranian Journal of Materials Science and Engineering, Vol. 21, Number 2, June 2024
RESEARCH PAPER

The Effect of PSi Pore Structure on the Characteristics of ZnO Rods Fabricated by Hydrothermal Method

R. Suryana[1,*], N. Usholihah[2], M. Diantoro[3]

* *rsuryana@staff.uns.ac.id*

[1,2] Department of Physics, Faculty of Mathematics and Natural Sciences, Universitas Sebelas Maret, Surakarta 57126, Central Java, Indonesia
[3] Department of Physics, Faculty of Mathematics and Natural Sciences, Universitas Negeri Malang, Malang 65145, East Java, Indonesia

Received: November 2023 **Revised: May 2024** **Accepted: May 2024**
DOI: 10.22068/ijmse.3431

Abstract: *Modifying photo-anode structures in DSSC devices is still challenging in improving efficiency. This study focused on the ZnO rod growth on several porous silicon substrates using the hydrothermal method and determining which porous silicon is appropriate for DSSC applications. The materials used for the growth solution were $Zn(NO_3)_26H_2O$ 0.05 M and $C_6H_{12}N_4$ 0.25 M. The hydrothermal process was carried out at 90°C for 6 h and then annealed at 450°C for 30 min. SEM revealed that PSi pore influences the structure, diameter, and density of ZnO rods. ZnO structures formed in ZnO rods with a dominant vertical growth direction, ZnO rods with an intersection direction, and flower-like ZnO rods. The diameter of the PSi pore affected the density of ZnO rods grown on the PSi. The average diameter size and the density of ZnO rods vary from 747.66-1610.68 nm and 0.22-0.90 rod/μm^2. XRD confirmed the presence of ZnO hexagonal wurtzite, Si cubic, and SiO_2 monoclinic. UV-Vis spectrometry characterization results showed that sample reflectance was influenced by ZnO rod density and PSi pitch. The larger density of ZnO rods and the smaller pitch of the PSi pore will lead to lower reflectance. In addition, band gap values were obtained in the 3.06-3.75 eV range. FTIR identified the existence of a ZnO vibration bond, indicating that ZnO was successfully grown on all PSi substrates. The ZnO rods grown on P15S1180 are expected to have more appropriate properties among all five samples for DSSC photoanode.*

Keywords: *ZnO like-flower, Hydrothermal, Reflectance, Porous silicon, ZnO rods.*

1. INTRODUCTION

Solar cells convert light into electrical energy through the photovoltaic (PV) effect [1]. Compared to other types of solar cells, Dye-Sensitized Solar Cells (DSSC) have cheap and simple production processes, are environmentally friendly, and have high efficiency (10-14.7%) [2]. However, DSSC still needs to improve its efficiency in being commercialized. Therefore, some research has been carried out to increase the efficiency of DSSC, one of which is by modifying the structure and morphology of the photoanode material [3].

Titanium dioxide (TiO_2) and Transparent Conducting Oxide (TCO) are commonly used photoanode materials. However, TiO_2 has low electron mobility and high electron-hole recombination, thus limiting the further development of DSSC [4]. Therefore, Zinc Oxide (ZnO) is an alternative material because of its good charge carrier mobility, higher exciton binding energy, stability, and diverse morphology [5]. But, DSSC-based ZnO has lower efficiency (2%) compared to DSSC-based TiO_2 (11.1%) [6]. So, ZnO is modified as nanostructures, such as in the following studies [7]. Photoanode material using Indium Tin Oxide (ITO) and ZnO nanorods has a higher efficiency of 4.45%, and photoanode material using Porous Silicon (PSi) and ZnO nanoparticles has an efficiency of 15.60% [8, 9]. The following research shows that the different substrates and ZnO structure will affect DSSC efficiency.

Photoanodes require a large surface area for the dye attached and good electron transport capabilities. ZnO has varied morphological structures, such as nanoparticles, nanowires, and nanorods. Compared to other structures, the structure of nanorods will provide a direct pathway for electrons to across semiconductor material. Moreover, the nanorods structure has a large surface area for the dye to attach, facilitating increased photogeneration of electrons upon light exposure to the DSSC [7, 10]. So, ZnO nanorods can improve photoanode electron transfer and surface area for dye adsorption [11]. The substrate material is essential in determining nanostructure

[DOI: 10.22068/ijmse.3431]

growth's structural, physical, and mechanical characteristics [12]. The substrate commonly used for ZnO nanorods growth is TCO [13]. However, TCO has a higher cost and limited thick modification. Therefore, this work will use silicon substrate due to wide surface modification, such as pore addition through the synthesis process. The pore in PSi can replace the role of the seed layer as a nucleation site, which helps maximize lattice matching between substrates and nanorods and ensure the vertical orientation of ZnO nanorods [14]. In addition, PSi can be used as an anti-reflective (AR) layer, which can increase photon absorption [15].

The ZnO rods characteristic is determined by the synthesis method. The Chemical Vapor Deposition (CVD) method can produce good crystal quality, but the synthesis process requires expensive costs and high temperatures (more than 450°C). The electrochemical deposition method has a cheap cost, easy to set up, and is a fast process. However, producing good ZnO nanorod crystal quality is difficult due to the low synthesis temperature. Among other synthesis methods, the hydrothermal method is suitable for ZnO rod growth because it is cheap and uses low temperatures. The hydrothermal method produces good enough ZnO rod crystal quality. After hydrothermal, the annealing process can be carried out at 300-500°C to improve the crystal quality [16]. In this study, the PSi used is commercialized PSi. ZnO rods with five pore variations will be synthesized using the hydrothermal method on PSi substrates. This study focuses on determining the effect of pore structure on the ZnO rod growth. This information will help determine which pore variations are appropriate for the photoanode material application.

2. EXPERIMENTAL PROCEDURES

The porous Silicon (PSi) used in this work was commercial PSi from Smart Membranes, Germany. PSi used has five pore variations: sample 1 (P15S155: pitch 1.5 µm; diameter 1 µm; depth 55 µm), sample 2 (P15S1180: pitch 1.5 µm; diameter 1 µm; depth 180 µm), sample 3 (P15S1200: pitch 1.5 µm; diameter 1 µm; depth 200 µm), sample 4 (P42S25200: pitch 4.2 µm; diameter 2.5 µm; depth 200 µm), and (e) sample 5 (P12S6220: pitch 12 µm; diameter 6 µm; depth 220 µm). ZnO rods were synthesized by hydrothermal technique on the PSi substrates, shown in Figure 1.

Zinc nitrate hexahydrate [$Zn(NO_3)_26H_2O$] 0.05 M and hexamethylenetetramine ($C_6H_{12}N_4$) 0.25 M were individually dissolved in the DI water for 1 h at room temperature. After that, each solution was mixed into one and stirred for 1 h.

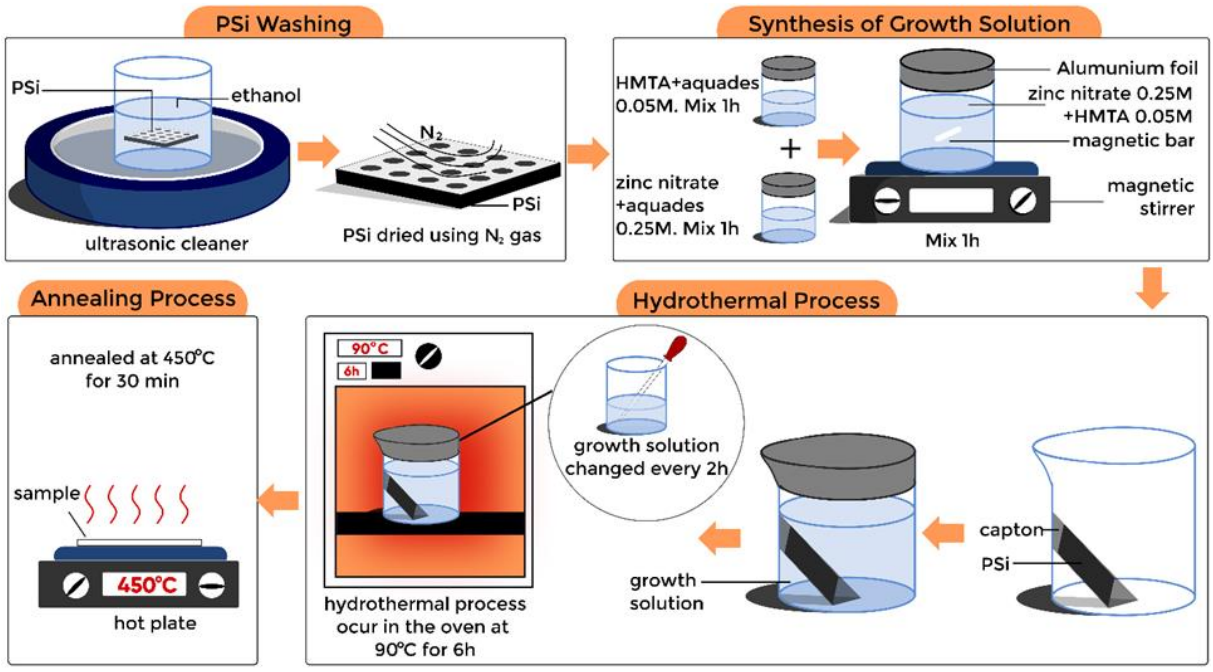

Fig. 1. ZnO fabrication process by hydrothermal method

[DOI: 10.22068/ijmse.3431]

The PSi substrates were cleaned using an ultrasonic cleaner for 1 min. The PSi substrates were leaned on the crucible wall with an angle of 45°, then immersed in a growth solution and covered with aluminum foil. The crucible was placed in an oven at a temperature of 90°C for 6 h. The growth solution was changed every 2 h. After 6 h, samples will be cleaned using ethanol and DI water. After that, samples were annealed on the hot plate at a temperature of 450° for 30 min. Scanning Electron Microscopy (SEM) (FEI Quanta-250) was used to observe ZnO rod morphologies. ZnO rod structures were characterized using X-ray diffraction (XRD) (Bruker D8 Advance). The sample's reflectance was observed using a UV-Vis Spectrophotometer (Analytik Jena 200 plus). Attenuated Total Reflectance-Fourier Transform Infrared (ATR-FTIR) (Bruker) determines the chemical bond on PSi surfaces.

3. RESULTS AND DISCUSSION

Morphologies of ZnO rods grown on the different PSi substrates using the hydrothermal method have been analyzed with SEM, as shown in Figure 2. Samples 1, 2, and 3 have the same diameter and pitch (1.5 μm and 1 μm) with different pore depth (55 μm, 180 μm, 200 μm). The ZnO rods grown on sample 1 are mostly vertically aligned, as shown in Figure 2(a). The ZnO rods grown on sample 2 have a flower-like structure, as shown in Figure 2(b). Meanwhile, the ZnO rods grown on sample 3 partially formed flowers and intersected each other, as shown in Figure 2(c). The diameter and density of ZnO rods can be seen in Table 1. Sample 1 has the largest diameter with the smallest density, followed by samples 3 and 2, respectively. Meanwhile, Figure 2 (d, e) shows ZnO rods grown on the different PSi pore diameters, pitches, and depths. The ZnO rods grown on sample 4 mostly form flowers, and the other rods intersect. The ZnO rods grown on sample 5 have structures that mostly intersect each other. The diameter and density of samples 4 and 5 ZnO rods can also be seen in Table 1.

In the early stages of the hydrothermal process, ZnO particles can be densely localized on PSi pores. After forming an adequate core density, ZnO rods will grow based on the nuclei formed [17]. Not all ZnO rods grow vertically, but some have specific growth directions or intersect each other [18]. During the heating process in the hydrothermal method, particles will meet to form an agglomeration of nanoparticles. These nanoparticles will provide nucleation sites in various directions so that ZnO rods will be created following different growth orientation directions [19]. On PSi substrates, flower-like structures can form when several ZnO rods on the pores gather and form flower-like structures. Several ZnO rods are joined at a central point [20].

Sample ZnO rod growth mechanism during the hydrothermal process on the different pores depth can be explained in Figure 3. Samples with different PSi pore depths have varied structures, diameters, and densities. The smaller pore depth will make ZnO particles quickly enter and stick to the bottom pore surface. This will make adequate core density easier to achieve and more nuclei formed. At the pore depth of 55 μm, sample 1 (Figure 3(a)), so many ZnO nuclei were formed. However, the number of nuclei formed is not matched by the pore's surface area availability. Therefore, several squeezed nuclei will quickly merge into one and fill the pore space. ZnO rods formed along the vertical direction with the largest diameter of all samples because the PSi pore can no longer accommodate ZnO particles attached to the ZnO nuclei. At the pore depth of 180 μm, sample 2 (Figure 3(b)), many nuclei formed because ZnO particles easily entered and stuck to the pore wall. The number of ZnO nuclei is balanced with a larger surface area, so between one nucleus to another still has a distance. Therefore, ZnO particles will attach to nuclei with different growth orientation directions, forming ZnO rods with the smallest diameter. Some of these ZnO rods will intersect to form a flower-like structure from the central point of the intersection. Compared to the pore depth of 200 μm, sample 3 (Figure 3(c)), the ZnO particles entering the pore are more challenging to achieve an adequate core density due to the large depth. This condition will form fewer ZnO nuclei, so the incoming ZnO particle will focus on sticking to the fewer nuclei. This condition will form a larger ZnO rod diameter than sample 2, which has more ZnO nuclei. A smaller pore depth will make more nuclei form, and the more nuclei formed will make the diameter of ZnO rods smaller. This condition can occur in samples 2 and 3. However, at too small pore depths, such as sample 1, ZnO nuclei close to each other in the same pore will

[DOI: 10.22068/ijmse.3431]

merge because the surface area is limited compared to samples 2 and 3. The diameter and density of ZnO rods that keep increasing during the growing process will allow several ZnO to merge so that ZnO rods will form a larger diameter than other samples [20].

Table 1. Diameter and density of ZnO rods grown on PSi

	Sample 1 (P15S155)	Sample 2 (P15S1180)	Sample 3 (P15S1200)	Sample 4 (P42S25200)	Sample 5 (P12S6220)
Diameter [nm]	1610.68±24.68	747.66±2.87	1379.86±6.61	793.17±6.04	989.34±15.50
Density [rod/μm^2]	0.22 ± 0.05	0.90 ± 0.23	0.30 ± 0.08	0.58 ± 0.15	0.71 ± 0.18

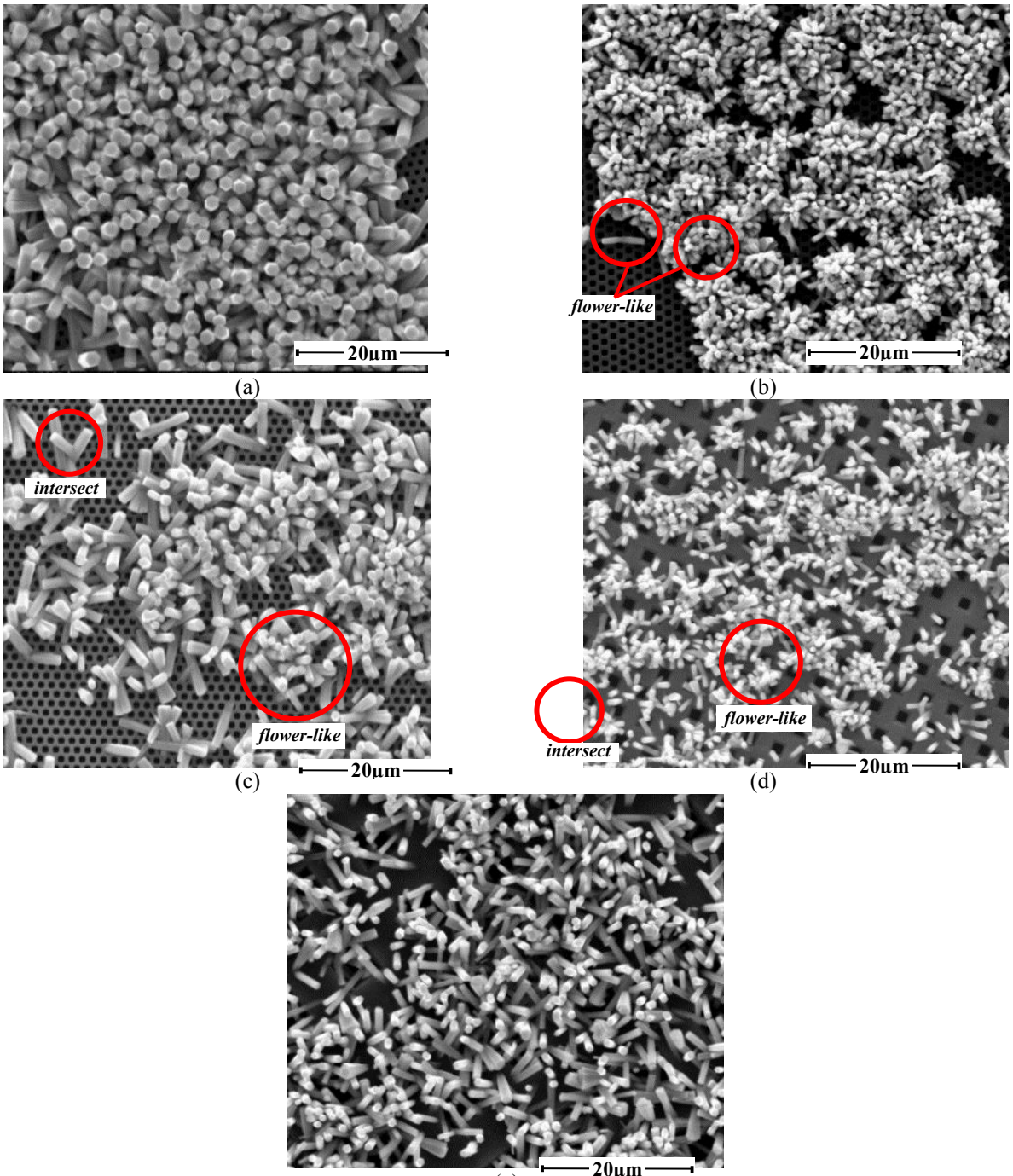

Fig. 2. SEM images (Top-view) of ZnO rods grown on PSi substrates

[DOI: 10.22068/ijmse.3431]

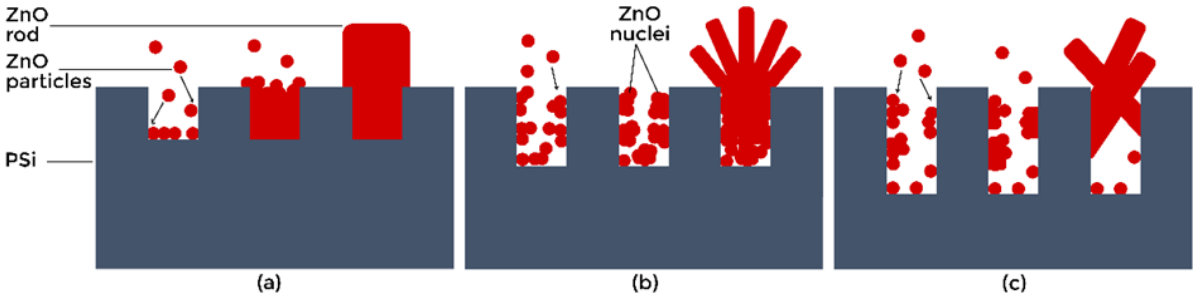

Fig. 3. ZnO rods growth mechanism on the different PSi pore depths: (a) Sample 1 (55µm); (b) Sample 2 (180µm); (c) Sample 3 (200 µm)

The effect of pore diameter and pitch can be determined by comparing ZnO rods grown in samples 3 and 4 with the same pore depth (200 µm). The diameter of ZnO rods in sample 3 (1379.86 nm) is larger than in sample 4 (793.17 nm). Meanwhile, the density of ZnO rods in sample 3 (0.30 rods/µm^2) is smaller than in sample 4 (0.58 rods/µm^2). PSi with the same pore depth but a larger pore diameter will make ZnO particles enter and stick to the pore wall easily. The larger pore diameter of sample 4 makes the pore surface area of sample 4 larger than that of sample 3. This condition will form more ZnO nuclei in sample 4 because there is enough space between the nuclei so that the nuclei are not close to each other, and the possibility of the ZnO nuclei merging is slight. A large number of nuclei formed leads to denser ZnO rods and smaller diameters, as seen in Table 1. PSi pore depth, diameter, and pitch in sample 5 are larger than in sample 4. Corresponding to the theory above, the ZnO rod diameter in sample 5 is larger than in sample 4.

Meanwhile, the density of sample 5 is larger than the density of sample 4. Sample 5 has a broader pore diameter which can provide much potential for ZnO rods to grow compared to sample 4. This result proves that ZnO rods only grow on PSi pores, not on the pitch.

XRD defined the crystalline structure of synthesized ZnO rods. Figure 4 shows the XRD pattern of ZnO rods grown on PSi substrates. Match! software identified the XRD spectrum using reference numbers 96-210-7060 for ZnO, 96-901-1057 for Si, and 96-412-4042 for SiO_2. The peaks indicating the hexagonal wurtzite ZnO rods phase appear at 2θ values of 31.88°, 34.58°, 36.39°, 47.74°, and 63.15° included in the reflection of (100), (002), (101), (012), (013). The crystal orientation ZnO of (130) did not appear in samples 2 and 3. The peaks of 2θ for Si cubic are 33.07° and 69.38° which have a crystal orientation of (211) and (422), and 2θ for SiO_2 monoclinic are 21.40°, 23.37°, 28.08°, 33.75°, 54.95°, 56,60°, 62.10° which have a crystal orientation of (001), (240), (060), (170), (391), (262), (800). The crystal orientation SiO_2 of (170), (391), and (800) did not appear, and (060) only appeared in sample 5. The SiO_2 layer forms when the Si surface reacts with oxygen molecules in the ZnO during synthesis [17].

For all samples, (100), (002), and (101) peaks of ZnO show the highest intensity. The better crystallite growth of the ZnO rod structure on PSi will have the narrower full half maximum (FWHM). The crystallite size (D) of the ZnO rod structure can be determined by using the Scherrer formula, as shown in equation (1).

$$D = \frac{K\lambda}{\beta \cos\theta} \quad (1)$$

Where k is a constant value of 0.94, λ is X-ray wavelength (1.5424 Å), β is FWHM, and θ is Bragg diffraction angle [15]. The crystallite size D of ZnO rods grown on PSi can be calculated using Equation (1) in Table 2. The largest crystallite size belongs to sample 5, and the smallest belongs to sample 3.

The tendency of crystal orientation to the crystallite size in each sample can be identified in Figure 5. Figure 5 (a-c) shows the crystallite size on orientation planes of (100), (002), and (101). Samples 1, 2, and 5 tend to the orientation plane of (002). Samples 3 and 4 tend to the orientation plane of (100). Figure 5 (d) shows all samples' average crystallite sizes ($\overline{D}$). Sample 5 has the largest crystallite size, followed by samples 4, 2, 1, and 3. Figure 6 shows the UV-Vis reflection spectra of the ZnO rod grown on the different pores of PSi. At wavelengths of 200 nm to 400 nm, samples have reflectance above 40%.

[DOI: 10.22068/ijmse.3431]

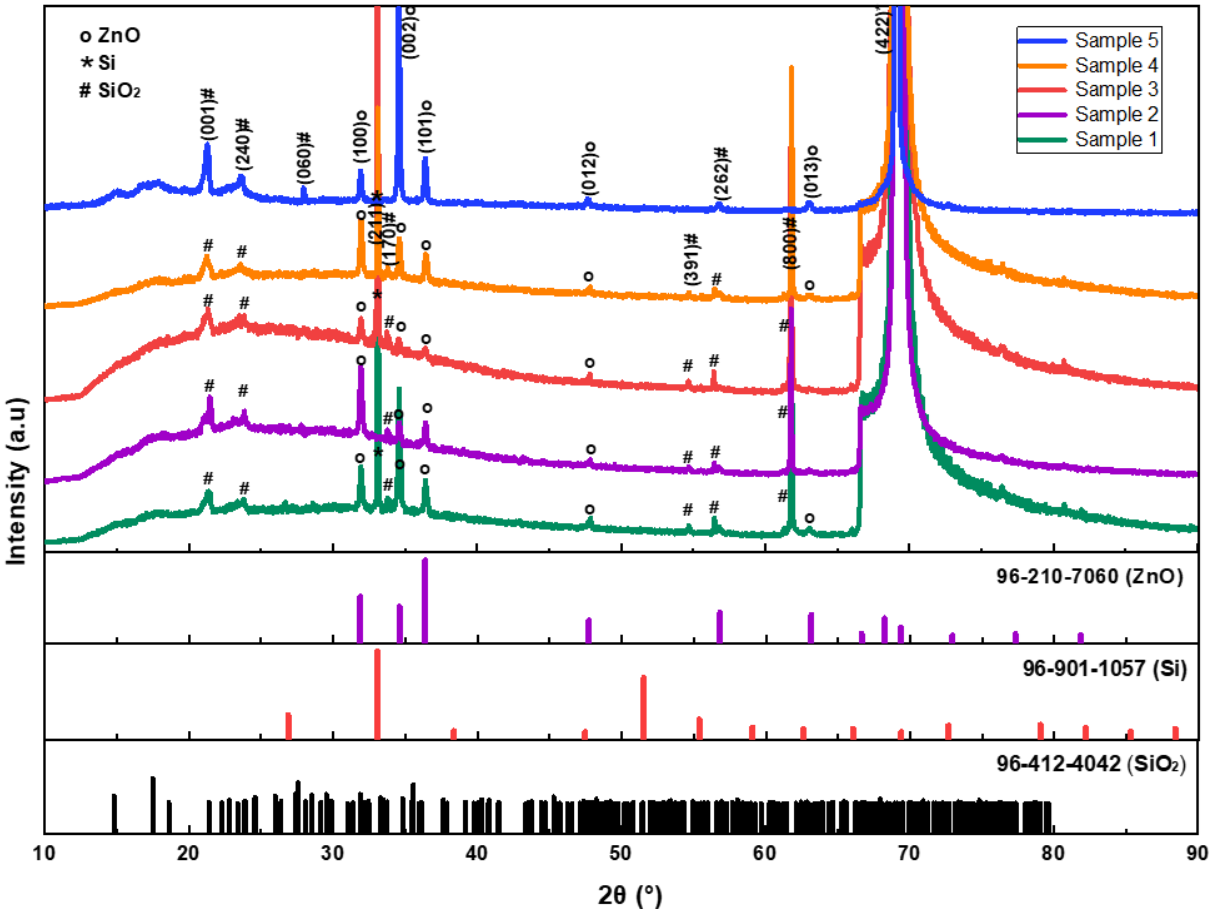

Fig. 4. XRD spectrum of the ZnO rods grown on PSi

Table 2. The crystallite size of ZnO rods grown on PSi

Crystal Orientation	Crystallite Size (D)					
	Sample 1 (P15S155)	Sample 2 (P15S1180)	Sample 3 (P15S1200)	Sample 4 (P42S25200)	Sample 5 (P12S6220)	$\bar{D}$ [nm]
(100)	38.99 ± 2.04	38.36 ± 2.47	37.83 ± 1.13	41.82 ± 1.03	40.11 ± 1.55	39.42 ± 1.65
(002)	39.58 ± 0.75	38.48 ± 5.44	31.56 ± 2.63	41.49 ± 1.48	46.78 ± 2.41	39.58 ± 2.54
(101)	35.98 ± 1.55	38.09 ± 6.90	36.44 ± 2.81	34.42 ± 1.32	39.41 ± 0.99	36.87 ± 2.72
$\bar{D}$ Sample [nm]	38.18 ± 1.45	38.31 ± 4.94	35.28 ± 2.19	39.24 ± 1.27	42.10 ± 1.65	

While at the wavelength of 400 nm to 1100 nm , samples have reflectance below 40%. The reflectance of all 5 samples is influenced by the amount of ZnO rods grown on PSi substrates and the PSi pore pitch. If the density of ZnO rods is larger, more light will be absorbed so that less light will be reflected [9]. Sample 2 has the lowest reflectance with the largest density of all samples, 0.90 rod/μm^2. It is followed by samples with the same diameter and pitch, namely samples 3 and 1, with densities of 0.30 rod/μm^2 and 0.22 rod/μm^2, respectively. However, this does not match the results in samples 3 and 4, which have the same pore depth. The density of sample 4, 0.58 rod/μm^2, is greater than the density of sample 3, 0.30 rod/μm^2, but the reflectance of sample 4 is greater than the reflectance of sample 3.

This result is because the pitch of sample 4 is greater than sample 3, so the incoming light will hit and be reflected. So, from these results, it can be concluded that pitch size also affects sample reflectance in addition to the density of ZnO rods. The reflectance of sample 4 is greater than sample 5 because there are fewer ZnO rods grown in sample 4 compared to sample 5. UV-Vis Diffuse Reflectance Spectroscopy (DRS) can also be used to determine bandgap energy (Eg) values (Figure 7) using the Kubelka-Munk equation as shown in equation (2).

[DOI: 10.22068/ijmse.3431]

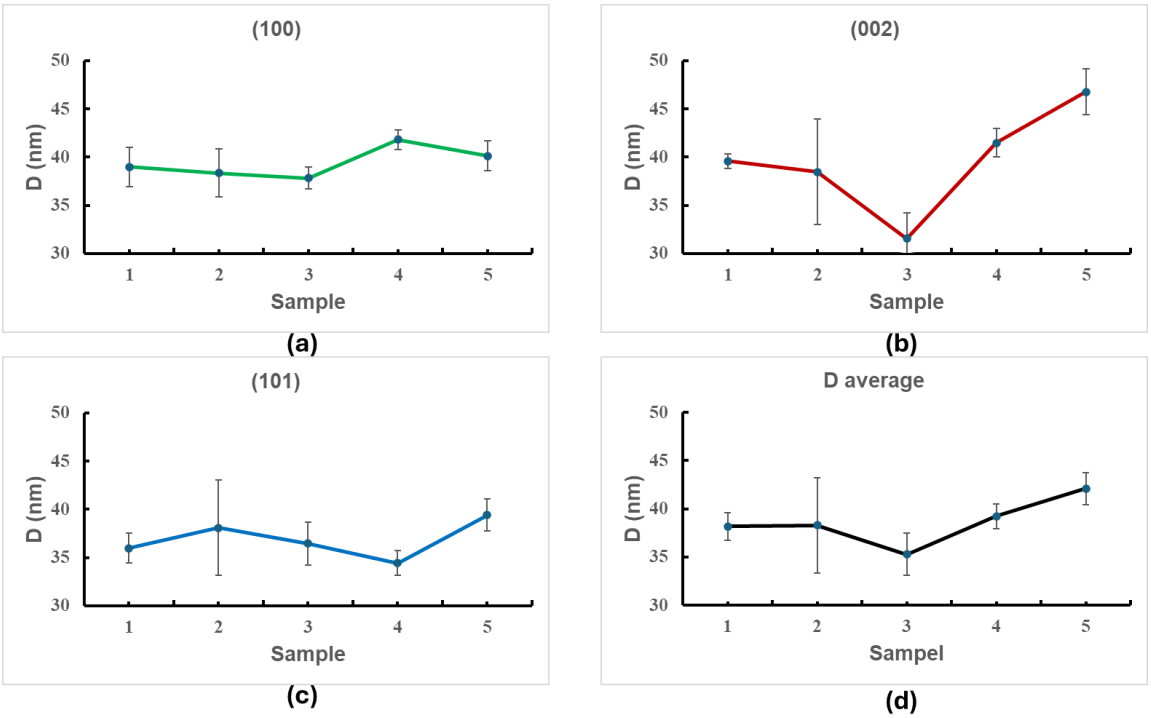

Fig. 5. Crystallite size (D) graph by orientation plane (a) (100), (b) (002), (c) (101), and (d) Average crystallite size (D) graph

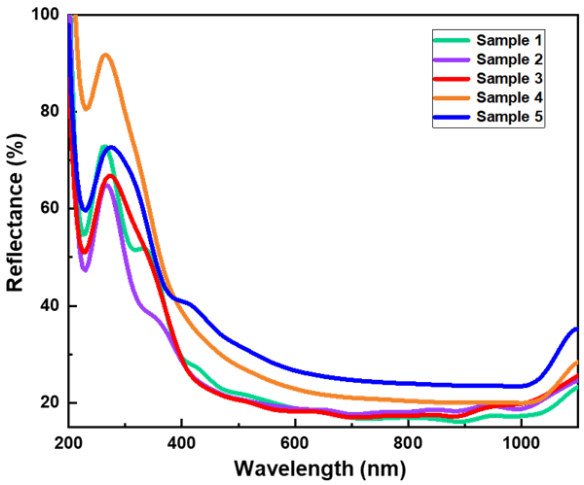

Fig. 6. UV-Vis reflection spectra of the ZnO rods grown on PSi

$$F(R) = \frac{k}{s} = \frac{(1-R)^2}{2R} \quad (2)$$

Where k is absorption K-M, s is the scattering coefficient, and R is the reflectance value [21]. Eg values are presented in Table 3. Sample 2 has the largest Eg value, followed by samples 4, 5, 3, and 1. The band gap energy of ZnO rods can depend on the length and diameter of the rods [4]. The varying Eg value is related to the quantum confinement effect due to the reduced size of the ZnO rods [14, 22]. Based on the results obtained, it can be seen that the Eg value will increase with the decrease in ZnO rod diameter size.

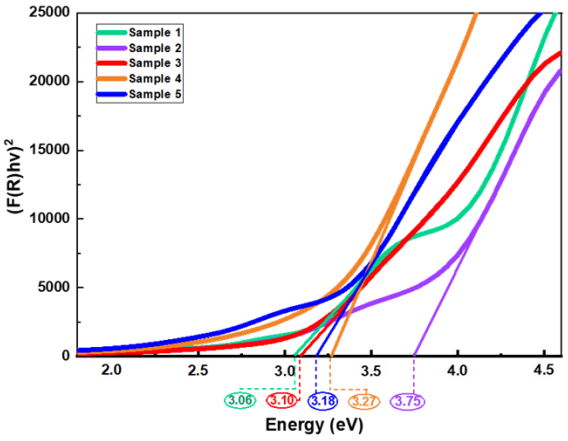

Fig. 7. Kubelka-Munk graph for bandgap energy (Eg) calculation of the ZnO rods grown on PSi

Table 3. Bandgap energy (Eg) value and diameter size of ZnO rods grown on PSi

	Sample 1 (P15S155)	Sample 2 (P15S1180)	Sample 3 (P15S1200)	Sample 4 (P42S25200)	Sample 5 (P12S6220)
Eg [eV]	3.06 ± 0.01	3.75 ± 0.01	3.10 ± 0.01	3.27 ± 0.01	3.18 ± 0.01
Diameter [nm]	1610.68 ± 24.68	747.66 ± 2.87	1379.86 ± 6.61	793.17 ± 6.04	989.34 ± 15.50

[DOI: 10.22068/ijmse.3431]

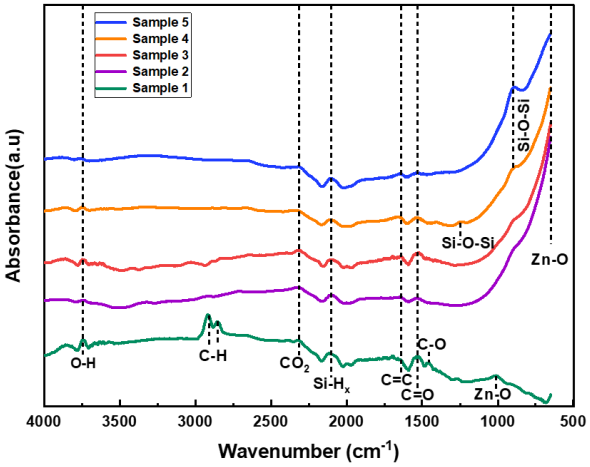

Fig. 8. FTIR spectrum of ZnO rods grown on PSi

Fourier Transform Infrared (FTIR) spectroscopy determines the chemical bonds formed during the synthesis process of ZnO rod growth on PSi. FTIR spectrum of ZnO rod growth on the PSi substrates is shown in Figure 8. FTIR spectra of the sample observed at 1010.83 cm^{-1} for sample 1 and 649.79 cm^{-1} for samples 2, 3, 4, and 5 are assigned to ZnO stretching vibration [23, 24]. For all samples, FTIR spectra observed at 3739.81 cm^{-1}, 2309.42 cm^{-1}, 2106.90 cm^{-1}, 1533.59 cm^{-1}, and 1646.51 cm^{-1} are assigned to stretching vibration of O-H, the absorption peak of CO_2, stretching vibration of Si-H_x, stretching vibration of C=O, and stretching vibration of C=C [25-28]. For sample 1, FTIR spectra of stretching C-H were observed at 2850.04 cm^{-1} and 2914.50 cm^{-1}, and stretching C-O at 1453.03 cm^{-1} [29, 30]. Stretching vibration of Si-O-Si was observed at 888.41 cm^{-1} and 1240.58 cm^{-1} for samples 4 and 5 [31, 32].

Sample 2, ZnO rods grown on P15S1180, is expected to have more appropriate properties among all five samples. Sample 2 has the highest bandgap energy (3.75 eV), which is expected to increase the efficiency of DSSC [9]. ZnO flower-like can work as good photoanodes due to their internal light-scattering ability, which has increased the electron transport rate [7]. The ZnO flower-like morphology also can provide a larger surface area in contact with the active layer and promote higher light absorption [9]. Sample 2 has the smallest diameter and the largest density of ZnO. This will lead to a larger surface area due to the flower-like structure having space in each rod compared to vertically ZnO, such as sample 1. A large surface area can improve dye adherence on the surface and electrolyte loading in the structure. This structure can improve the layer's light scattering effect and light absorption [19].

4. CONCLUSIONS

ZnO rods were successfully grown on PSi using the hydrothermal method at a temperature of 90°C for 6 h. SEM images show that the different PSi pores influence the structure, diameter, and density of ZnO rods grown. The different pore depths will affect the structure and diameter of ZnO rods. ZnO rods form vertically aligned, intersected each other, and flower-like structures. A smaller pore depth will make more nuclei form, and the more nuclei formed will make the diameter of ZnO rods smaller. This condition can occur in samples 2 and 3. However, at too small pore depths, such as sample 1, ZnO nuclei close to each other in the same pore will merge because the surface area is limited compared to samples 2 and 3. The different pore diameters and pitches will affect the density of ZnO rods. The wider diameter of the pore will provide much potential for ZnO rods to grow. This research also proves that ZnO rods only grow on PSi pores, not on the pitch. XRD results confirm the presence of ZnO hexagonal wurtzite, Si cubic, and SiO_2 monoclinic for all samples. UV-Vis spectrometry shows that ZnO rod density and PSi pore size influence the sample's reflectance. The band gap energy varies from 3.06-3.75 eV. The larger density of ZnO rods and the smaller pitch of the PSi pore will lead to lower reflectance and the larger pore pitch. FTIR confirms that ZnO successfully grows on all PSi substrates through a ZnO vibration bond. This research is expected to be useful for DSSC photoanode material development in future research.

ACKNOWLEDGEMENT

This work was supported by the Ministry of Education, Culture, Research, and Technology, Indonesia, for its financial support through the PDUPT 2023 program (contract number 055/E5/PG.02.00.PL/2023).

REFERENCES

[1]. Noorasid, N. S., Arith, F., Alias, S. N., Mustafa, A. N., Roslan, H., Johari, S. H., Rahim, H. R. A. and Ismail, M. M.,

[DOI: 10.22068/ijmse.3431]

Synthesis of ZnO Nanorod Using the Hydrothermal Technique for Dye-Sensitized Solar Cell Application, Intelligent Manufacturing and Mechatronics, Lecture Notes in Mechanical Engineering, eds. M. Bahari, S., Harun, A., Zainal Abidin, Z., Hamidon, R. and Zakaria. S., Springer, Singapore, 2021, 895-905.

[2]. Kandasamy, M., Murugesan, S., Selvaraj, M. and Alam, M. M., "Aminosilicate Modified Zinc Oxide Nanorod-GO Nanocomposite for DSSC Photoanodes." Ceram. Int., 2022, 48, 6037-6045.

[3]. Sufyan, M., Mehmood, U., Gill, Y. Q., Nazar, R. and Khan A. U. H., "Hydrothermally Synthesize Zinc Oxide (ZnO) Nanorod as An Effective Photoanode Material for Third-Generation Dye-sensitized Solar Cells (DSSC)." Mater. Lett., 2021, 297, 130017.

[4]. Chamanzadeh, Z., Ansari, V. and Zahedifar, M., "Investigation on the Properties of La-Doped and Dy-Doped ZnO Nanorods and Their Enhanced Photovoltaic Performance of Dye-Sensitized Solar Cells." Opt. Mater., 2021, 112, 1-8.

[5]. Nikhil, S. K., Das, M. Kumar, A., Bhagavathiachari, M. and Nair, R. G., "Effect of Aspect of C-Axis Oriented ZnO Nanorods on Photoelectrochemical Performance and Photoconversion Efficiency." Opt. Mater., 2021, 121, 1-7.

[6]. Mohiuddin, O., Obaidullah, M. and Sabah, C., "Improvement in Dye Sensitized Solar Cells from Past to Present." Opt. Quantum Electron., 2018, 50, 1-28.

[7]. Jamalullail, N., Mohamad, I. S., Norizan, M. N., Mahmed, N. and Nadia, B., "Recent Improvements on TiO_2 and ZnO Nanostructure Photoanode for Dye Sensitized Solar Cells : A Brief Review." EPJ Web Conf., 2017, 162, 01045.

[8]. Shirvani, M. and Naji, L., "Comparative Study on The Electrochemical Synthesis of Zinc Oxide Nanorods Using Chronoamperometry and Chronopotentiometry and Their Application in Inverted Polymer Solar Cells." Colloids Surf. A: Physicochem. Eng., 2023, 660, 130889.

[9]. Abood, M. K., Fayad, M. A., Al Salihi, H. A. and Salbi, H. A. A., "Effect of ZnO Nanoparticles Deposition on Porous Silicon Solar Cell." Materials Today: Proceedings, 2021, 42, 2935.

[10]. Nandi, P. and Das, D., "Morphological Variations of ZnO Nanostructures and Its Influence on The Photovoltaic Performance When Used as Photoanodes in Dye Sensitized Solar Cells." Sol. Energy Mater Sol. Cells, 2022, 243, 1-10.

[11]. Lin, L. Y., Yeh, M. S., Lee, C. P., Chou, C. Y., Vittal R. and Ho K. C., "Enhanced Performance af A Flexible Dye-Sensitized Solar Cell With A Composite Semiconductor Film of ZnO Nanorods and ZnO Nanoparticles." Electrochim. Acta, 2012, 62, 341-347.

[12]. Aydemir, G., Utlu, G. and Çetinel, A., "Growth and Characterization of ZnO Nanostructures on Porous Silicon Substrates: Effect of Solution Temperature." Chem. Phys. Lett., 2019, 737, 1-7.

[13]. Yadav, S. C., Sharma, A., Devan, R. S. and Shirage, P. M., "Role of Different Counter Electrodes on Performance of TiO_2 Based Dye-Sensitized Solar Cell (DSSC) Fabricated with Dye Extracted from Hibiscus Sabdariffa as Sensitizer." Opt. Mater., 2022, 124, 1-9.

[14]. Mosalagae, K., Murape, D. M. and Lepodise, L. M., "Effects of Growth on Properties of CBD Synthesized ZnO Nanorods Grown on Ultrasonic Spray Pyrolisis Deposited ZnO Seed Layers." Heliyon, 2020, 6, 1-10.

[15]. Rosli, N., Halim, M. M. and Hashim, M. R., "Growth of ZnO Microstructure on Porous Silicon." Solid State Phenomena, 2019, 290, 261-266.

[16]. Le, A. T., Ahmadipour, M. and Pung, S. Y., "A Review on ZnO-Based Piezoelectric Nanogenerators: Synthesis, Characterization Techniques, Performance Enhancement, and Applications." J. Alloys Compd., 2020, 844, 156172.

[17]. Dalvand, R., Mahmud, S. and Rouhi, J., "Direct Growth of Flower-Like ZnO Nanostructures on Porous Silicon Substrate

[DOI: 10.22068/ijmse.3431]

Using A Facile Low-Temperature Technique." Mater. Lett., 2015, 160, 444-447.

[18]. Yang, D., Ramu, A. G., Lee, Y., Kim, S., Jeon, H., Sathishkumar, V. E., Al-Mohaimeed, A. M., Al-Onazi, W. A., Algarni, T. S. and Choi, D., "Fabrication of ZnO Nanorod Based Gas Sensor Pattern by Photolithography and Lift Off Techniques." J. King Saud Univ. Sci., 2021, 33, 1-8.

[19]. Yuliasari, F., Aprilia, A. and Hidayat, R., "Improved Dye-Sensitized Solar Cell Performance With Hedgehog-Like Shaped ZnO Nanorod Grown Using ZnO Nanoparticles Seed Layer." Material Today: Proceedings, 2022, 52, 248-251.

[20]. Kim, I., Viswanathan, K., Kasi, G., Thanakkasaranee, S., Sadeghi, K. and Seo, J., "ZnO Nanostructures in Active Antibacterial Food Packaging: Preparation Methods, Antimicrobial Mechanisms, Safety Issues, Future Prospects, and Challenges." Food Rev. Int., 2022, 38, 537-565.

[21]. George, P. and Chowdhury, P., "Complex Dielectric Transformation of UV-Vis Diffuse Reflectance Spectra for Estimating Optical Bandgap Energies and Materials Classification." The Analyst, 2019, 144, 3005-3012.

[22]. Ahmad, A., Khan, S., Khan, M., Luque, R., Jalalah, M. and Alsaiari, M. A., "Microwave Assisted Preparation of Barium Doped Titania (Ba/TiO_2) As Photoanode in Dye Sensitized Solar Cells." Appl. Sci., 2022, 12, 1-11.

[23]. Dole, B. N., Mote, V. D., Huse, V. R., Purushotham, Y., Lande, M. K., Jadhav, K. M. and Shah, S. S., "Structural Studies of Mn Doped ZnO Nanoparticles." Curr. Appl. Phys., 2011, 11, 762-766.

[24]. Praseptiangga, D., Zahara, H. L., Widjanarko, P. I., Joni, I. M. and Panatarani, C. "Preparation and FTIR Spectroscopic Studies of SiO_2-ZnO Nanoparticles Suspension for The Development of Carrageenan-Based Bio-Nanocomposite Film." AIP Conf. Proc., Solo, Indonesia, 2020, 2219, 100005.

[25]. Karthik, K. V., Raghu, A. V., Reddy, K. R., Ravishankar, R., Sangeeta, M., Shetti, N. P. and Reddy, C. V., "Green Synthesis of Cu-Doped ZnO Nanoparticles and Its Application for Photocatalyst Degradation of Hazardous Organic Pollutants." Chemosphere, 2022, 287, 132081.

[26]. Kumaraswamy, S., Babaladimath, G., Badalamoole G. and Mallaiah, S.H., "Gamma Irradiation Synthesis and In Vitro Drug Release of ZnO/PVA Hydrogel Nanocomposites." Adv. Mater. Lett., 2017, 8, 546-555.

[27]. Rahmani, A., Remache, L., Guendouz, M., Aida, M.S. and Hebbol, Z., "Impact of The Meso-Psi Substrate on ZnO Thin Films Deposited by Spray Pyrolysis Technique for UV Photodetectors." Appl. Phys. A, 2021, 127, 396.

[28]. Raja, K., Ramesh, P.S. and Geetha, D., "Structural, FTIR and Photoluminescence Studies of Fe Doped ZnO Nanopowder by Co-Precipitation Method." Spectrochim. Acta A Mol. Biomol. Spectrosc., 2014, 131, 183-188.

[29]. Kumar, B., Smita, K., Cumbal, L. and Debut, A., "Green Approach of Fabrication and Application of Zinc Oxide Nanoparticles." Bioinorg. Chem. Appl., 2014, 2014, 1-7.

[30]. Tokumoto, M. S., Briois, V., Santilli, C. V. and Pulcinelli, S. H., "Preparation of ZnO Nanoparticles: Structural Study of The Molecular Precursor." J. Sol-Gel Sci. Technol., 2003, 26, 547-551.

[31]. Abdullah, A., Haider, A. and Jabbaar, A., "Fabrication of Porous Silicon as A Gas Sensor: The Role of Porous Silicon Surface Morphology." J. Appl. Sci. Nanotechnol., 2020, 2, 35-42.

[32]. Khashan, K. S., "Optoelectronic Properties of ZnO Nanoparticles Deposition on Porous Silicon." Int. J. Mod. Phys. B, 2011, 25, 277-282.

[DOI: 10.22068/ijmse.3431]